

Current Materials Research Using X-Rays and Related Techniques III

Selected peer-reviewed full text papers from the
10th International Conference on
X-Rays and Related Techniques in Research
and Industry (ICXRI 2021)

Edited by

Muhamad Faiz Md Din
Fakhroul Ridzuan Hashim
Nazrul Fariq Makmor
Muhammad Azwadi Sulaiman
Norazharuddin Shah Abdullah
Wan Fahmin Faiz Wan Ali
Nik Akmar Rejab

Current Materials Research Using X-Rays and Related Techniques III

Selected peer-reviewed full text papers from the
10th International Conference on
X-Rays and Related Techniques in Research
and Industry (ICXRI 2021)

Edited by
Muhamad Faiz Md Din
Fakhroul Ridzuan Hashim
Nazrul Fariq Makmor
Muhammad Azwadi Sulaiman
Norazharuddin Shah Abdullah
Wan Fahmin Faiz Wan Ali
Nik Akmar Rejab

Current Materials Research Using X-Rays and Related Techniques III

Selected peer-reviewed full text papers from the
10th International Conference on
X-Rays and Related Techniques in Research
and Industry (ICXRI 2021)

Selected peer-reviewed full text papers from the
10th International Conference on
X-Rays and Related Techniques in Research and Industry
(ICXRI 2021), August 18-19, 2021,
Kuala Lumpur, Malaysia (virtual online)

Edited by

**Muhamad Faiz Md Din, Fakhroul Ridzuan Hashim,
Nazrul Fariq Makmor, Muhammad Azwadi Sulaiman,
Norazharuddin Shah Abdullah,
Wan Fahmin Faiz Wan Ali and Nik Akmar Rejab**

Copyright © 2022 Trans Tech Publications Ltd, Switzerland

All rights reserved. No part of the contents of this publication may be reproduced or transmitted in any form or by any means without the written permission of the publisher.

Trans Tech Publications Ltd
Kapellweg 8
CH-8806 Baech
Switzerland
<https://www.scientific.net>

Volume 908 of
Key Engineering Materials
ISSN print 1013-9826
ISSN web 1662-9795

Full text available online at <http://www.scientific.net>

Distributed worldwide by

Trans Tech Publications Ltd
Kapellweg 8
CH-8806 Baech
Switzerland

Phone: +41 (44) 922 10 22
Fax: +41 (44) 922 10 33
e-mail: sales@scientific.net

Preface

This conference is organized to provide an opportunity to all individuals and organizations who are involved and interested in the advancement of materials characterization techniques to share their views and experiences. Additionally, ICXRI2021 provides a platform for exchanging information, discussing scientific problems and findings, and fostering friendship and partnership. Materials characterization techniques have contributed extensively to research and services.

The progress in material science, solid-state physics, catalysis, biomedicine and pharmacology, and other fields have benefited much from these techniques. With the recent evolution of computing power, improved software and digital systems, enhanced capabilities, and greater precision handling, these techniques have gained much interest and have greatly widened their application in many new fields for rapid, economical, and on-the-mark analysis. Thus, it is timely to have this conference to assess current developments, deliberate on recent innovations, and introduce new ideas that will spur future trends and applications for these techniques.

Organizing Committee

Patron

Lt Jen Dato' Hasagaya bin Abdullah (Vice Chancellor, NDUM)

Advisor:

Brig Jen Prof. Ir Dr. Norazman bin Mohamad Nor (Deputy Vice Chancellor Research & Innovation, NDUM)

Prof. Dr. Zainal Arifin bin Ahmad (Chairman of XAPP-MNS)

Kol Assoc. Prof. Dr. Khairol Amali bin Ahmad (Dean of Faculty of Engineering, NDUM)

Chairman:

Assoc. Prof. Dr. Muhamad Faiz bin Md Din (NDUM)

Honorary Secretary:

Assoc. Prof. Dr. Khairul Nizar bin Ismail (UniMAP)

Prof. Dr. Fauziah binti Hj. Abdul Aziz (Vice-Chairman, XAPP-MNS)

Secretary:

Assoc. Prof. Dr. Fakroul Ridzuan bin Hashim (NDUM)

Assistant Secretary:

Dr. Anis Shahida Niza binti Mokhtar (NDUM)

Honorary Treasurer:

Dr. Hishamuddin bin Husain (Nuklear Malaysia)

Treasurer:

Mr. Ja'afar bin Adnan (NDUM)

Secretariat:

Assoc. Prof. Dr. Mohd Taufik bin Jusoh @ Tajudin
(NDUM)

Dr. Siti Aminah binti Mohd Noor (NDUM)

Dr. Wan Yusmawati binti Wan Yusoff (NDUM)

Dr. Fazilatulaili binti Ali (NDUM)

Dr. Latifah Sarah binti Supian (NDUM)

Scientific:

Assoc. Prof. Dr. Siti Nooraya binti Mohd Tawil
(NDUM)

Assoc. Prof. Dr. Khairul Rafezi bin Ahmad
(UNIMAP)

Assoc. Prof. Dr. Norazharuddin Shah bin Abdullah
(USM)

Dr. Wan Yusmawati binti Wan Yusoff (NDUM)

Dr. Ahmad Zahirani bin Ahmad Azhar (IIUM)

Dr. Roshanorlyza binti Hazan (Nuklear Malaysia)

Dr. Nik Akmar bin Rejab (USM)

Technical, Publicity & Website:

Assoc. Prof. Dr. Muhammad Azwadi bin
Sulaiman (UMK)

Dr. Shah Rizal bin Kasim (USM)

Mr. Mohd Hermas bin Ab Jalil (NDUM)

Mr. Muhammad Hakirin bin Roslan
(NDUM)

Mr. Roslan bin Husin (NDUM)

Exhibition & Competition:

Assoc. Prof. Dr. Hasan Zuhudi bin Abdullah
(UTHM)

Assoc. Prof. Dr. Ainun Rahmahwati binti
Ainuddin (UTHM)

Dr. Khairul Anuar bin Shariff (USM)

Dr. Wan Fahmin Faiz bin Wan Ali (UTM)

Dr. Ahmad Farid bin Azmi (NDUM)

Sponsorship:

Prof. Dr. Fauziah binti Hj. Abdul Aziz (Vice-Chairman, XAPP-MNS)
Prof. Dr. Ambar bin Yarmo (UKM)
Dr. Badrol bin Ahmad (Damascus)
Dr. Cik Rohaida binti Che Hak (Nuklear Malaysia)
Dr. Meor Yusoff Meor bin Sulaiman (Fenomena Inovasi (M) Sdn. Bhd.)
Mr. Ahmad Khairulikram bin Zahari (Nuklear Malaysia)
Mr. Wilfred@Sylvester Paulus (Nuklear Malaysia)

Protocol, Hospitality and Transportation:

Prof. Dr. Mohd Taufiq Ishak (NDUM)
Mr. Mohd Solehin Bin Mohd Nasir (NDUM)
Mr. Mohd Salman Bin Mohd Sabri (NDUM)
Mr. Nazrul Fariq Bin Makmor (NDUM)
Ms. Noor Fadzilah Binti Mohamed Sharif (NDUM)

Sponsors

Platinum Package



Gold Package



Silver Package



Table of Contents

Preface

Chapter 1: Polymers and Composites

Prediction and Optimization on Tribological Behaviour of Kenaf/Carbon Fiber Reinforced Epoxy Matrix Hybrid Composites S.N.M. Badari, N. Sariffudin, A. Ali, N.A.H. Sharuhil, F.D.M. Daud and H.H.M. Zaki	3
The Effect of Graphite Loading as Reinforcement on Carbon Foam from Natural Resources N.Z. Hassan, M.N. Mohamed Hatta, N.A. Badarulzaman and N.F. Mohd Joharudin	9
Synthesis and Characterization of Palm Kernel Oil Polyol Based Shape Memory Polyurethane: Effect of Different Diisocyanates N.A. Rasli @ Rosli and S.A. Zubir	14
Characterization of Sodium Alginate Membrane Plasticized by Polyols and Polyamine for DMFC Applications M.T. Musa, N. Shaari and S.K. Kamarudin	20
Effect of Chemical Treatment on Mechanical and Morphological Properties of Sugarcane Bagasse Reinforced Unsaturated Polyester Composite N.A. Zulkipli, S.H. Mohd, M.B. Abu Bakar, M. Mohamed and N.A.M. Rosdi	26
Effect of Graphene on Mechanical and Morphological Properties of Coconut Shell Reinforced Unsaturated Polyester Composite A. Abdullah, N.A.M. Rosdi, M.B. Abu Bakar, S.H. Mohd, N.H. Abdullah and M. Mohamed	33
UV Radiation Crosslinking of Acrylated Palm Olein (APO) Copolymer Resins for 3D Printing S.N.S.S. Ibrahim, M.U. Wahit, M. Talib, N. Othman, N.A. Shukri, F.F. Hilmi and M.A. Arshad	39
Surface Analysis of Grafted Low Density Polyethylene Film by FTIR and XPS Spectroscopy N.A. Shukri, Z. Ghazali, M.U. Wahit, F.F. Hilmi and S.N.S.S. Ibrahim	49
Box Behnken Design to Optimize Parameter for Vapor Grafting of Cinnamaldehyde Essential Oil onto Polyvinyl Alcohol F.F. Hilmi, M.U. Wahit, Z. Ghazali, N.A. Shukri and S.N.S.S. Ibrahim	54
Radiation Modification of Commercial Polyvinylidene Fluoride (PVDF) Backsheet Film for Mechanical and Thermal Properties Enhancement M.F. Shaharudin, N.A. Shukri, S.N.S.S. Ibrahim, M.F.N. Abd Lah, N.A.F. Othman, M.H. Muhammad Sayuti and N.I. Soh	62
Physiochemical Properties of Biofilm from <i>Dioscorea hispida</i> Starch Blended with Glycerol Extracted from Recycling Cooking A. Adila, A.H.Z. Aimi, N.F. Shoparwe and M.R.S. Fatimah	68
Crystallinity of Nanocellulose and its Application in Polymer Composites: A Short Review N.A. Rejab, J.O. Akindayo and M. Mustapha	74
Characterization of Thin Film PLA/PBAT Reinforced with Microcrystalline Cellulose Derived from <i>Gigantochloa albociliata</i> M.R.S. Fatimah, N.H. Jusoh, A.A. Rahim, T.D.O.R. Krishnan and N.F.M. Rawi	80
Study on Composition of Rice Husk Silica Reinforcement to Hardness and Microstructure of Recycling Milled AA7075 N.F.M. Joharudin, N.A. Latif, M.S. Mustapa, N.Z. Hassan and A. Supawi	86
<i>Tectona grandis</i>: Examine an Ultrastructure on Cultivated Teakwood due to the Scanning Electron Microscopy Enhanced by Heat Treatment M.S. Sulaiman, R. Wahab, N. Mokhtar, T. Edin and S.M. Razali	92
Correlation of Humidity and Mechanical Properties of Different Grades of RT-PMMA M.J. Norazrina, M.A. Firdaus and P. Longere	105
Influence of Gamma-Irradiation on Swelling Percentage, Flammability Resistance and Morphological Analysis of EPDM/Sepiolite Composites M.Z. Nurul Aizan, I. Hanafi, R. Arjulizan and I. Sofian	110

Chapter 2: Materials for Biomedical Application and Pharmacology

Porous NiTi Shape Memory Alloy Fabricated via Powder Metallurgy Technique Using Pore Forming Agent	
N.A. Abd Kadir, H.H.M. Zaki, J. Abdullah, F.D.M. Daud and N. Sariffudin	119
Effect of Sintering Temperature on Hardness of Bioactive Glass/Cordierite	
A.K. Fakhruddin and H. Mohamed	125
Characterizations of Calcium Oxide from Calcined Eggshell Waste	
M. Khalid, S.S. Jikan, S. Adzila, Z.M. Yunus and N.A. Badarulzaman	130
Effect of Soaking Time on the Compositional and Morphological Changes of DCPD-Coated β-TCP Bioceramic	
N.Z. Zaidi, N.R. Ridzwan, A.H.M. Mohammed and K.A. Shariff	135
Synthesis and Characterization of Sol-Gel Derived Strontium Doped S53P4 Bioglass	
T.T. Swe, H. Mohamad, K.A. Shariff and K. Ishikawa	141
Preliminary Study on the Bioactivity Properties of Cordierite/β-Wollastonite Biocomposite Ceramics	
H. Ismail and H. Mohamad	148
Effect of Calcium Salt Coating on Cordierite Powders on Bioactivity Properties	
T.N.I. Tuan Ab Rashid and H. Mohamad	154
Extraction and Characterization of Natural Hydroxyapatite from Black Tilapia Fish Bone for Biomedical Applications	
S.K. Dermawan, Z.M.M. Ismail, M.Z. Jaffri and H.Z. Abdullah	159
Characterization of the Halal Natural Hydroxyapatite Extract from Black Tilapia Fish Scale	
M.Z. Jaffri, H.Z. Abdullah, Z.M.M. Ismail and S.K. Dermawan	165
Effect of Stirring Speed on the Formation and Characteristic of Alginate Microspheres via Gelation/ Emulsification Method	
T.T.U. Nguyen, Z.A.A. Hamid and A. Nurazreena	171
Fabrication and Characterization of Alginate/Iron (III) Oxide Beads and Biofilm for Biomedical Applications	
W.A.M.A. Zakhi and M.I. Idris	177

Chapter 3: Ceramics

Influence of Feldspar Addition on the Properties of $\text{CaCu}_3\text{Ti}_4\text{O}_{12}$ Ceramic	
A.S. Juhari, S.M. Sharifuddin, F.A.M. Pabli, J.J. Mohamed, Z.A. Ahmad, M.F. Ain and M.A. Sulaiman	185
Effect of Pressure Load on the Physical Properties of ZTA-TiO_2-Cr_2O_3	
H. Manshor, A. Ali and A.Z.A. Azhar	190
Comparative Study on the Wears of ZTA-TiO_2-Cr_2O_3 Ceramic Cutting Tool and Commercial Ceramic Cutting Tool	
R.N. Mudzaffar, H. Manshor, A.Z.A. Azhar, N.A. Rejab and A. Ali	196
The Effects of MWCNT Addition to Physical Properties of ZTA-MgO Cutting Tool	
N.E. Hamidon, H. Manshor, A.Z.A. Azhar, N.A. Rejab and A. Ali	202
The Effect of Polyvinyl Alcohol Addition on the Solid Carbon Infusion in Zirconia-Toughened Alumina	
N. Roshidan, H. Manshor, A.N. Rozhan and A.Z.A. Azhar	208
Dielectric Properties of Low Concentration Barium Doped $\text{K}_{0.5}\text{Na}_{0.5}\text{NbO}_3$ Lead Free Ceramics Prepared via Solid State Reaction Method	
J.J. Mohamed, M.Q. Saari, F.K. Bahanuridin, M.F. Ab Rahman, M.H. Jumali and A.H. Yuwono	223
Densification of Zirconia Toughened Alumina Added CeO_2 Ceramics via Hot Isostatic Press Sintering Technique	
N.K. Su, N.A. Rejab, Z.A. Ahmad and N.S. Abdullah	228
Compressive Strength of Zirconia-Toughened Alumina (ZTA) Foam with CaCO_3 and CeO_2 Addition via Polymeric Sponge Replication Technique	
N.A. Rejab, A.R. Jamaludin, N.S. Abdullah and Z.A. Ahmad	234

Development and Characterisation of Triaxial Electrical Porcelains from Malaysian Ceramic Minerals	
H. Yahya, A. Ahmad, M.A.A. Abdul Aziz and M. Selamat	240
Preparation of Porous Porcelain with Treated Flue Gas Desulfurization (FGD) Sludges the Foaming Agent	
S.I. Alias, B. Johar, S.N.F. Adam, M.A.A. Taib, F.F. Othman and H. Yahya	245
 Chapter 4: Materials and Technologies for Opto- and Microelectronics	
Optical and Structural Properties of Controlled pH Variation on Zinc Oxide Nanostructured via Hydrothermal Method	
A. Ali, A. Nadiyah, T.P. Ter, J. Hidayani, A. Syamsir and M.L. Rahimi	253
Light Absorption Enhancement Using Graphene Quantum Dots and the Effect of N-719 Dye Loading on the Photoelectrode of Dye-Sensitized Solar Cell (DSSC)	
N.F.M. Sharif, M.Z.A. Ab Kadir, S. Shafie, M.F. Md Din, Y. Yusuf and B. Samaila	259
TiO₂ Photoelectrode Band Gap Modification Using Carbon Quantum Dots (CQDs) for Dye-Sensitised Solar Cells (DSSCs)	
N.F.M. Sharif, S. Shafie, M.Z.A. Ab Kadir, M.F. Md Din, Y. Yusuf and S. Shaban	265
Growth of Nanostructured Zinc Oxide on Flexible Conductive Substrate: A Review	
A. Ainun Rahmahwati, S.S.M. Ismail, K. Zakiah, R. Hussin and I.S. Aida	271
Interfacial Reaction between SAC3807 Lead-Free Solders and Different Copper Substrate via Reflow Soldering Process	
M.R. Fauzi, N.A. Amiruddin, S.A. Osman, R.A.M. Anuar and M.S. Hashim	278
Physical and Electrochemical Properties of Graphene Decorated with ZnO Hollow Spheres for Supercapacitor Applications	
A.L.A. Abdullah, S. Radiman, M.A.A. Hamid and M.F.Y.M. Hanappi	284
Evaluation of Olivine LiFePO₄ Polyanionic Cathode Material Using Density Functional Theory	
S.I. Ahmad, F.W. Badrudin, A.L.A. Abdullah, M.Z.A. Yahya, M.F.M. Taib and O.H. Hassan	293
The Effect of Oxygen and Air Flow on the Characteristic of Zinc Oxide ZnO Nanorods	
N.M. Ahmed and T.A. Tabet	299
Ionizers as Major ESD Countermeasure in 12nm Gate Oxide Semiconductor Manufacturing	
N.F. binti Abd Ghani, M.Z. bin Bakhri, I. bin Mohamadiah, K.A. bin Ahmad and A.S.N. binti Mokhtar	308
 Chapter 5: Functional Materials	
Comparison of Stability Mechanism of Graphene Nanoparticles in Polyester Oil	
M.A. Saufi and H. Mamat	319
Structural Behaviour and Electrical Properties of a Ball Milled MnCoGe Compounds	
A.R.B.A. Rahman, M.F. Md Din, N.S. Suhaimi, S.N. Mohd Tawil, J.L. Wang, N.H. Idris and M. Ismail	326
The Effect of Annealing Temperatures on the Phase Transition and Structural Properties of MnCoGe Compound	
A.R.B.A. Rahman, M.S. Mohd Sabri, M.F. Md Din, N.S. Suhaimi, J.L. Wang, N.H. Idris and M. Ismail	332
Influence of Annealing Temperatures on the Structural Behaviour and Electrical Properties of La(FeSi)₁₃ Alloys	
M.I. Zulkifly, N.F. Makmor, A.R.B.A. Rahman, F.R. Hashim, M.F. Md Din and W.F.H. Wan Zambri	337
Electrical Properties and Raman Scattering of Palm Oil Based Carbon Nanotube	
N.S. Suhaimi, M.F. Md Din, C.Y. Tan, M.T. Ishak, A.R.B.A. Rahman, W.F.H. Wan Zambri and J.L. Wang	343
Fabrication and Characterization of Nickel Oxide Nanofibers by Electrospinning Technique	
S.S.Z. Abidin, L.Y. Jian, K.K. Ying, M. Muslimin, N.U. Saidin and N.M. Zali	348

Chapter 6: Materials and Technologies in Environmental Engineering

Catalytic Oxidative Desulfurization of Model Diesel Using TBHP-DMF System N.A.S. Mohd Nazmi, S.J.M. Rosid, N. Mohd Shukri and W.N. Wan Abdullah	355
Identification of <i>Nymphoides indica</i> and <i>Eichhornia crassipes</i> as Potential Plants for the Phytoremediation of Batik Wastewater C.Y. Wah, M.A. Sulaiman, S.M. Sharifuddin, C.S. Xian and N.S. Subki	361
Optimization Study of Malachite Green Dye Adsorption by Eggshell Using Response Surface Methodology H.M. Hoo, M. Mohamad, R. Wannahari, M.N. Masri, T.P. Ter and N.A. Mohidem	367
High Purity Nano-Silica from Rice Husk Ash (RHA) via Chemical Method as Additive/Stabilizing Agent for CO₂ Capture Application M.S. Mahmud, F.D.M. Daud, N. Sariffudin, H.H. Mohd Zaki, N.H. Nordin and N.F. Mohammad	373
Adsorption Isotherm Analysis for CO₂ Capture Using Barium Oxide Impregnated Iron(III) Oxide by Ultrasonic-Assisted Synthesis A.H. Lahuri, M.A. Yarmo, M.N. Abu Tahari and N. Dzakaria	379
Response Surface Methodology Optimization of Chemical Oxygen Demand Removal by Rice Husk Activated Carbon L.K. Vin, R. Mohd Ghazi, N.R. Nik Yusoff and M. Jani	385
Controlled Process of Radiation-Induced Grafting by Chemical Vapour Deposition for the Synthesis of Metal Adsorbent N.A.F. Othman, S. Selambakkannu and T.A. Tuan Abdullah	392
Properties of Polyethersulfone Ultrafiltration Membrane by Incorporating Ionic Liquid for Humic Acid Removal A.S. Che Miur, N.F. Shoparwe, Z.A. Abdul Hamid, M.Z. Makhtar and N.I. Zainuddin	400
Comparative Study of Fe,N-TiO₂ Photocatalysts under UV Light Irradiation Z. Malik, I.S. Aida, A.R. Ainuddin, R. Hussin and K. Zakiah	406
Physical Properties of γ Irradiated TiO₂ Nanoparticles M. Muslimin, S.S.Z. Abidin, N.M. Zali and N.U. Saidin	414
Characterizations of High Entropy Alloy Powder as Catalyst Synthesized by Mechanical Alloying for Azo Dye Degradation N.H. Abu Hassan, N.A. Zin, N.H. Shaari, N.A. Fadil, M.S. Jami and N.H. Nordin	419

Chapter 7: Materials and Technologies of Chemical Production

A Study on the Catalytic Technology for Reduction of Naphthenic Acid Compound from Acidic Crude Oil N. Mohd Shukri, W.A. Wan Abu Bakar, M.R. Russman and W.N. Wan Abdullah	429
Fermentable Sugar via Diluted Acid Hydrolysis of Sugarcane Bagasse S.K.E. Ab Rahim, H.A.P. Kasi and N.S. Abdullah	435
Effect of Ferrite as Filler in Sugarcane Bagasse Paper via Irradiation Method A.A. Azmi and S.A. OTHMAN	441
Effects of Sulphuric Acid and Speed Rotation on Hydrolysis of Bamboo Sawdust N.M. Zahir, M.K. Abdullah, N.A. Jabit and S. Ismail	448

Chapter 8: Structural Metals and Alloys

Phase Composition of Sintered AlCrFeNi J. Setiawan, S. Pribadi, A. Jamaludin, M.H.A. Hasa and D.H. Prajitno	457
Morphological and Structural Properties of Sn-Bi Lead-Free Solder in 6 M Potassium Hydroxide M.N. Masri, M.F. Sazali, M.F. Mohd Nazeri, A.A. Mohamad and T.P. Ter	462
Simulation and Experimental of Crack Propagation in Automotive Engineering Component A. Ali, M.K. Faidzi, K.H. Kamarudin, M.F. Abdullah and M.R. Saad	467
Detection of Vibration Induced Fatigue Crack Propagation Using a Hybrid Method M.F. Shamsudin and T.H. Gan	473

Chapter 9: Mineral Processing and Metallurgy

Microwave-Assisted Acid Digestion of Malaysian Monazite for Determination of REEs Using ICP-MS S. Udayakumar, N. Baharun and S.A. Rezan	481
Utilization of Empty Fruit Bunch Derived Vapor for Carbon Deposition within Iron Ores H. Marzuki, A.N. Rozhan and H. Purwanto	487
Malaysia's Rare Earth Element Story: Characterizing the "Amang" Z.A. Natasya and N.S. Abdullah	494
Recovery of Light Rare Earth Elements (LREE) from Monazite by Alkaline Fusion R. Hazan, H. Mohd Noor and K. Mohamed Takip	503
Extraction of Thorium Oxide (ThO₂) from Malaysian Monazite through Alkali Digestion: Physical and Chemical Characterization Using X-Ray Analysis C.R.C. Hak, Z. Januri, I. Mustapha and S. Mahat	509

Chapter 10: Laser Technologies

RSM Modeling and Validation of Glass Assisted Laser Micro Drilling of Silicon Wafer S. Sivarao, A. Ali, K.Z. Ku Ahmad and S. Pujari	517
RSM Modelling for Laser Cutting of Shore Wood to Replace Traditional Manufacturing Method S. Sivarao, A. Ali, K.Z. Ku Ahmad and S. Pujari	526

Chapter 11: Thin Films, Coatings and Surface Engineering

X-Ray Reflectivity Analysis in Evaluating Multilayer Thin Film Fabrication N.N. Samsudin, M.F. Omar and N.S.M. Rudin	537
Structural Analysis of DLC Thin Film Using X-Ray Reflectivity and Raman Spectroscopy Techniques K.A. Nadzari, M.F. Omar, N.S.M. Rudin and A.K. Ismail	543
Evaluation of Reduced Graphene Oxide Film Using In-Plane XRD Measurement N.S.M. Rudin and M.F. Omar	549
Influence of Electrophoretic Deposition (EPD) Voltage on SOFC Interconnect Morphology Y.N. Lowrance, M.A. Azmi, H.A. Rahman, N.F.A. Rahman, H. Zakaria and S. Hassan	555
Effect of Spherical Tungsten Carbide Load to the Corrosion Behaviour of Plasma Transfer Arc Hard Facing in Acidic and Alkaline Environment K. Zakiah, A.R. Ainuddin and M.N. Mohamed Hatta	563
Green Synthesis of Nanostructured Zinc Oxide (ZnO) - Titanium Dioxide (TiO₂) Thin Films R. Hussin, M.H. Razali, A.R. Ainuddin, K. Zakiah, I.S. Aida and Z. Harun	570
Corrosion Behavior of Antimony (Sb) Modified Galfan (Zn-Al) Coated Steel M.I. Ikhliluddin, M. Mohamad, M.A. Mat Yajid, E.M.N.E. Abu Bakar and W.F.F. Wan Ali	578
pH Effect on Microbial Corrosion by <i>Pseudomonas aeruginosa Sp.</i> on Galvanized JIS3502 Steel N.S. Azmi, N. Hasim, M.A. Mat Yajid, E.M.N.E. Abu Bakar, N. Nosbi, N.A. Rejab and W.F.F. Wan Ali	585
AlCrN Coated WC by PVD at Various Deposition Temperatures S. Rizali, C.L. Ling, A.F.A. Latif, U. Nur, M.A. Mat Yajid, N.S. Abdullah and W.F.F. Wan Ali	592
Effect of Complexing Agent on The Morphology and Corrosion Effect of Cu-Sn-Zn Ternary Alloy via Electroplating R. Rosley, S.S. Jikan, N.A. Badarulzaman, F. Esa, S.N. Ab Razak, M.S. Roslan and M. Khalid	598
Tropical Climate Adaptation via Biomimicry and Surface Functionalization for Electronic Circuitry N.N. binti Din and K.A. bin Ahmad	605
The Mechanical Integrity of Self-Healing Coating Embedded with Microencapsulated Vegetable Oil Z. Baharom, Z.M.M. Ismail, M.I. Idris and H.Z. Abdullah	612

Chapter 12: Building Materials

Compressive Strength of Concrete Bricks with Recycled Concrete Sludge Waste A.Z.A. Azhar, S.A. Saad, N.M. Shaffiar and M.Y. Ismail	621
Influence of Modified Chemical Compositions on Palm Oil Fuel Ash to the Physico-Mechanical Properties of Porcelain S.G. Durumin-Iya, M.Z. Noh and M.S. Adamu	626
Study of Different Composition of Gypsum as Retarder in Ordinary Portland Cement N.A.M. Khairuddin, F.E. Ja'afar, S. Ahmad and K.N. Ismail	633
Interfacial Transition Zone (ITZ) Study of Concrete with Polyethylene Terephthalate (PET) Plastic A.A. Omar, M.Z.H.A. Sabri and K.N. Ismail	639
Study of Fly Ash Concrete Exposed to Elevated Temperature M.Z.H.A. Sabri, R.A. Malek, A.A. Omar and K.N. Ismail	645
Mechanical Enhancement of Composite Bricks Using Kenaf and Oil Palm Cellulose Nanofibrils N.A.S. Shari, N.A. Mocktar, A. Mohamed Noor, M.Z.A. Aziz, M. Arifullah and M.K.A.A. Razab	651
Effect of Adding Hydrogen Peroxide (H₂O₂) and Sodium Dodecyl Sulphate (SDS) to the Properties of Fly Ash (FA)-Based Geopolymer Mortar M.A.Z. Aziz, A.Z. Norzeity, I. Johari and S.R. Kasim	658
Use of Municipal Solid Waste Incineration Bottom Ash and Rice Husk Ash as Blended Cement R. Che Amat, K.N. Ismail, N.M. Ibrahim, R.A. Malek and K.R. Ahmad	664
Phase Transformation of FGD By-Product into Plaster Mould via Heat Treatment Process F.F. Othman, B. Johar, K.S. Fhan, N.A. Rejab and S.I. Alias	672
Coal Power Plant Fly Ash Characterization Assessment for Geopolymerization Process N.W.A. Khairuddin, A.K. Zahari, E. Phillip and M.F. Sujan	678

CHAPTER 1:

Polymers and Composites

Prediction and Optimization on Tribological Behaviour of Kenaf/Carbon Fiber Reinforced Epoxy Matrix Hybrid Composites

Siti Norbahiyah Mohamad Badari^{1,a*}, Norshahida Sarifuddin^{1,b},
Afifah Mohd Ali^{1,c}, Nurul Atikah Hamdan Sharuhil^{1,d},
Farah Diana Mohd Daud^{1,e} and Hafizah Hanim Mohd Zaki^{1,f}

¹Department of Manufacturing and Materials Engineering, International Islamic University Malaysia, Jalan Gombak, 53100 Kuala Lumpur, Malaysia.

^{a*}norbahiyah@unimap.edu.my, ^bnorshahida@iium.edu.my, ^caffahali@iium.edu.my, ^datikah.sharuhil97@gmail.com, ^efarah_diana@iium.edu.my, ^fhafizahhanim@iium.edu.my

Keywords: DOE, ANOVA, Factorial design, Hybrid composite, Sliding wear, Coefficient of friction.

Abstract. The awareness on sustainability of the environment among the researchers leads to the exploration of natural fiber composite materials. Hybridization of synthetic fiber and natural fiber is one of the potential strategies to enhance the mechanical properties as well as the degradability of such composite materials. However, less information concerning the optimization of tribological properties of this hybrid composite is available in literature. The aim of this study is to propose a statistical model to predict and optimize wear and coefficient of friction of kenaf/carbon reinforced epoxy composite. The value of parameters; load and sliding velocity ranges from 10 to 30 N and 20.9 to 52.3 m/s, respectively, are used to assess wear and coefficient of friction (COF) of different stacking sequences using the Analysis of Variance (ANOVA). The tribological test was conducted using a pin-on-disc tribometer. Multifactorial design analysis was employed to optimize the test control variables. It was found that, the optimized factors that affects the coefficient of friction and wear is at load 30 N and sliding velocity of 52.36 m/s. The proposed statistical models for wear and COF have 99.5% and 97.6% reliability, respectively. The generated equation models are bounded within the wear test control factors and ranges. The outcome from this study will be very useful for main parameter prediction for an optimized wear and COF.

Introduction

In recent decade, polymer have risen as a promising advanced material in various applications for having attractive characteristics including light weight, easy to manufacture and cost effective. Henceforth, many significant studies were made to utilize polymers in many more industrial applications, using reinforcements that incorporated with the polymers in order to increase their mechanical and physical properties [1][2][3]. Later, fiber reinforced polymer matrix composites have become extensively attractive due to their properties such as lightweight, high strength, high stiffness and good coefficient of friction [4]. However, over the time, environmental awareness and regulations has increased and grown, opening ways for the development of ecofriendly and biodegradable reinforcement materials [5].

Natural polymer composites are environmentally friendly polymer composite as they were reinforced with natural element such as corn fiber, kenaf fiber, and palm ash compared to synthetic fiber such as glass and carbon fibers. Many studies have been conducted to reduce wear and friction by investigating different types of natural fiber composite for tribological applications [6][7][8][9]. Kenaf belongs to Malvacea family has been found to be an important source of fiber for composites with the potential to revolutionize industrial applications[10]. Significant global effort has been devoted to research, and funding's have been dedicated to its different stages of development, from a very basic scientific understanding to a proof-to-concept applications. The implementation of fibers from agricultural wastes as new reinforcement of polymer matrix composites is supposed to have a large potential in improving the tribological properties at an affordable cost [11]. Works is underway

to define standards and to predict procedures which will facilitate the deployment of kenaf fibers in its various forms into tribological applications.

Application of Design of Experiments (DOE) such as surface response, Taguchi and factorial has gained significance in providing evidence rank orders of the information on the influence of parameters and responses. Modelling is one of the effective tools for understanding the tribological properties of certain materials. The statistical Analysis of Variance (ANOVA) is a proven method used by researchers to investigate significant design parameter affects the tribological characteristic [12]. In this study, influences of combination factors of parameters such as applied load, sliding velocity and stacking configuration on optimal tribological behavior can be predicted and analyzed. In addition, regression analysis was used to derive the mathematical models of the control factors and their interactions.

Based on previous studies on wear and frictional behavior, it has been observed that several studies were carried out regarding the potential of kenaf fiber reinforced polymer composites in tribological applications [13-15]. However, there is limited study conducted on proposing wear and friction models, particularly for the kenaf fiber as reinforcement. Thus, the present study was carried out to propose statistical models for predicting wear and friction coefficient of the kenaf/carbon reinforced epoxy matrix hybrid composite using the ANOVA and regression analysis method.

Experimental Details and Methodology

Materials, Design Aspects and Fabrication Procedure. The sample material used for experimentation is kenaf/carbon reinforced epoxy (KCRE) hybrid composite. Kenaf and carbon were defined as ‘K’ and ‘C’ to indicate the stacking sequences. The properties of materials used for the fabrication of KCRE hybrid composites shown in Table 1. Two types of stacking sequence from carbon and kenaf fibers were fabricated using 40:60 (fiber: matrix ratio) consists of kenaf and carbon plies into 3mm thickness composite by vacuum infusion method. The samples were cut into 9 mm x 30 mm dimension for tribo testing (Fig. 1).

Table 1 Properties of materials used in the fabrication

Properties	Materials		
	Kenaf (K)	Carbon (C)	Epoxy Resin
Density [g/cm ³]	1.22	1.77	1.122
Tensile Strength [MPa]	200	1380-2070	78
Elongation at break (%)	1.6	1.5	4.5
Type	Fine fabric	2X2 Twill	Viscous liquid



Fig. 1 Types of KCRE composite pin stacking sequence
(a) CKCKC and (b) CCKCC.

Tribological Testing. A wear test was performed using a pin on disc tribometer under dry sliding condition following ASTM standard (ASTM G99). The wear test conditions are according to the parameters in Table 2. The KCRE composite pin with dimension of 9 mm x 30 mm was mounted vertically on the tester arm facing the rotating abrasive surface. The actual test placement is shown in Fig. 2.

Table 2 Wear test conditions

Parameters	Operating condition
Fiber content [vol%]	40%
Sliding time	600s
Temperature	Room temperature
Surface condition	Dry
Pin material	KCRE
Disc material	400 SC
Track diameter	0.025m

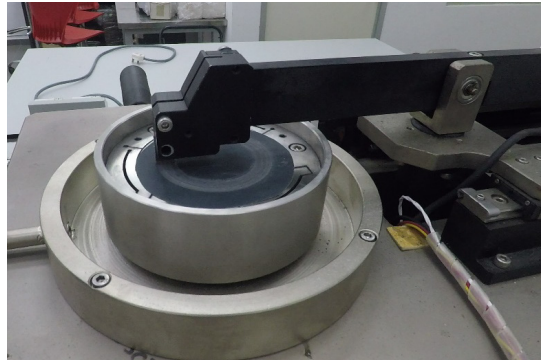


Fig. 2 Actual KCRE composite pin placement on the pin on disc tribometer.

An average of steady state COF was taken into analysis. The wear rate of the pin was recorded by measuring the mass of the pin before and after the wear test. The wear rate was then calculated by Eq. 1.

$$w = V_{loss}/(W \times L) \quad (1)$$

Where w is the wear rate in [$\text{mm}^3/\text{N.m}$], V_{loss} is the volume loss in [mm^3], W is the applied load in [N], and L is the sliding distance in [m].

Analysis of Variance (ANOVA). The results of wear rate and COF from the tribological testing were tabulated in multifactorial design with wear test control variables within level range (Table 3) for two types of stacking sequence, CKCKC and CCKCC. The design parameters were set according to the factor variables with type and ranges of values (Table 4). Analysis of variance (ANOVA) is used to summarize the experimental data using Design Expert software.

Table 3 Wear test control variables and corresponding levels

Control variables	Level		
	Low	Medium	High
Load [N]	10	20	30
Sliding velocity [m/s]	20.94	36.65	52.36

Table 4 Design parameters at different levels for all stacking sequences

Load (N)	Sliding velocity (m/s)
10	20.94
20	36.65
30	52.36

Results and Discussion

Analysis of variance (ANOVA). Wear and COF resultants are affected by frictional parameters. Experimentally, it is a time-consuming procedure to study the effects of an individual parameter on wear and COF. ANOVA analysis based on F-value is applied to the developed model to assess the importance for wear and coefficient of friction as shown in Table 5 and Table 6 respectively. Higher the F-value indicates that alteration in output can be explained by a developed model and the associated P-value is also used to determine, whether 'F' is adequate to direct a statistical significance. The P-values below than 0.05 indicate that the developed model and the terms are significant.

Table 5 Results of ANOVA for wear.

Source	Sum of Squares	F-Value	P-Value
Model	1.345E-10	701.32	<0.001
A: Stacking sequence	1.777E-11	1204.05	<0.001
B: Load	5.879E-11	1991.90	<0.001
C: Sliding velocity	5.149E-11	1744.63	<0.001
Residual error	5.903E-13		
Lack of fit	5.903E-13		

Table 6 Results of ANOVA for coefficient of friction

Source	Sum of Squares	F-Value	P-Value
Model	1.25	125.99	<0.001
A: Stacking sequence	0.0405	53.13	<0.001
B: Load	0.7913	518.88	<0.001
C: Sliding velocity	0.1122	147.10	<0.001
Residual error	0.0305		
Lack of fit	0.0305		

The values of statistical correlation coefficients, 'R-square', 'adjusted R-square' and 'predicted R-square', shows the accuracy of the statistical model. The value of statistical correlation coefficients for wear and COF is shown in Table 7. The 'R-square' value provides the fraction of total alteration in the output expected by developed model. Given that 0.9956 and 0.9762 proves a good fit to data. The value of 'adjusted R-square' giving a good correlation between predicted and actual for wear and COF, 0.9942 and 0.9684 respectively. The 'predicted R-square' value for the model is 0.9920 and 0.9566, indicates an excellence prediction to the actual value of wear and COF respectively.

Table 7 Statistical correlation coefficients

Control variables	Wear	COF
R-square	0.9956	0.9762
Adjusted R-square	0.9942	0.9684
Predicted R-square	0.9920	0.9566

Statistical Analysis Model. The experimental output data related to wear rate and coefficient of friction was used to develop a statistical model, which relates significant input parameter to required output. The ANOVA analysis suggests a model correlates the investigation data with responses in a quadratic model for wear and COF are given by Eq. 2 and Eq. 3 respectively.

$$\begin{aligned}
 \text{Wear} = & 3.666E - 06 + 5.736E - 07 \times \text{Stacking sequence} - 9.651E - 07 \times \text{Load} \\
 & + 1.449E - 06 \times \text{Load} + 1.292E - 06 \times \text{Sliding velocity} \\
 & - 2.226E - 07 \times \text{Sliding velocity} - 1.836E - 07 + 2.811E \\
 & - 07 \times \text{Stacking sequence} \times \text{Load} + 2.890E \\
 & - 07 \times \text{Stacking sequence} \times \text{Sliding velocity}
 \end{aligned} \tag{2}$$

$$\begin{aligned}
 \text{COF} = & 0.4543 + 0.0274 \times \text{Stacking sequence} + 0.1359 \times \text{Load} + 0.0222 \times \text{Load} \\
 & + 0.0779 \times \text{Sliding velocity} + 0.0021 \times \text{Sliding velocity} \\
 & - 0.0106 \times \text{Stacking sequence} \times \text{Load} + 0.0464 \times \text{Stacking sequence} \times \text{Load} \\
 & - 0.0429 \times \text{Stacking sequence} \times \text{Sliding velocity} \\
 & + 0.0216 \times \text{Stacking sequence} \times \text{Sliding velocity} \\
 & - 0.0631 \times \text{Load} \times \text{Sliding velocity} + 0.0371 \times \text{Load} \times \text{Sliding velocity} \\
 & - 0.0017 \times \text{Load} \times \text{Sliding velocity} + 0.0124 \times \text{Load} \times \text{Sliding velocity}
 \end{aligned} \tag{3}$$

The equations can be used to predict responses for given levels of each control factor. Therefore, this equations of predicting value of wear and COF can be used effectively for combination of load, sliding velocity and stacking sequence. The equation gives predicted values within the ranges of input parameters.

Optimization. The main aim of this study is to minimize wear rate and COF. In order to achieve this, optimization analysis by Multifactorial model design was carried out. The outcome result suggests the most desired factors between load, sliding velocity and stacking sequence shown in Table 8. Optimum factors are found to be CKCKC stacking sequence, load of 30 N and sliding velocity of 52.36 m/s with 90.7% desirability. From the observation, under all stacking configurations, KCRE composites showed decrement of wear and COF as load and sliding velocity increases. This shows that kenaf fiber assisted in reducing wear during sliding. Kenaf fiber is found to be able to form an effective protective layer, a back film transfer, consisting of wear debris at higher load and sliding velocity[13]. Significant amount of back film transfer assisted in enhancing the wear and frictional performance of KCRE composites [14].

Table 8 Response optimization and desirability

Source	Minimum	Optimum
A: Stacking sequence	CCKCC	CKCKC
B: Load (N)	10	30
C: Sliding velocity (m/s)	52.36	52.36
Desirability		0.907

Conclusion

On basis of evidence presented in this investigation, some important findings are given as:

1. Multifactorial design analysis shows that the optimal combination of input parameters within the range of load, sliding velocity and stacking sequence are 30 N, 52.36 m/s and CKCKC configuration respectively.
2. The proposed statistical models for wear and coefficient of friction have 99.5% and 97.6% reliability, respectively. These model can be very useful for material pre-fabrication procedure to avoid failures occurring.

Acknowledgement

The authors would like to express the gratitude to the Ministry of Higher Education (MOHE) of Malaysia for the support through the awarded grant no (FRGS 17-033-0599), Kuliyyah of Engineering International Islamic University Malaysia (IIUM), and also to Research Management Centre (RMC) IIUM for facilitating this project.

References

- [1] V. K. Thakur, M. K. Thakur, and R. K. Gupta, Review : raw natural fiber – based polymer composites, *Int. J. Polym. Anal. Charact.*, 19:3 (2014), 256-271.
- [2] H. Ku, H. Wang, N. Pattarachaiyakoop, and M. Trada, A review on the tensile properties of natural fiber reinforced polymer composites, *Compos. B. Eng.*, 42:4 (2011), 856–873.
- [3] B. Barari, T. K. Ellingham, I. I. Qamhia, K. M. Pillai, L. Turng, and R. Sabo, Mechanical characterization of scalable cellulose nano-fiber based composites made using liquid composite molding process, *Compos. B. Eng.*, 84 (2016), 277-284.
- [4] D. K. Rajak, D. D. Pagar, P. L. Menezes, and E. Linul, Fiber-reinforced polymer composites: manufacturing, properties, and applications, *Polym.*, 11(10) (2019):1667.
- [5] O. Faruk, A. K. Bledzki, H. Fink, and M. Sain, Biocomposites reinforced with natural fibers : 2000 – 2010, *Prog. Polym. Sci.*, 37:11 (2012), 1552–1596.
- [6] A. Erdemir, Solid lubricants and self-lubricating films, In: Bhushan, B., (ed.) *Handb. Mod. Tribol.*, CRC Press, Boca Raton, 2001, pp. 787–818.
- [7] R. Gujjala, S. Ojha, S.K. Acharya and S.K. Pal, S.K., Mechanical properties of woven jute–glass hybrid-reinforced epoxy composite, *J. Compos. Mater.*, 48 (2014), 3445 - 3455.
- [8] T. Mukherjee and N. Kao, PLA based biopolymer reinforced with natural fibre: a review, *J Polym Environ*, 19 (2011), 714–725.
- [9] E. Omrani, P. L. Menezes, and P. K. Rohatgi, State of the art on tribological behavior of polymer matrix composites reinforced with natural fibers in the green materials world, *Eng. Sci. Technol. an Int. J.*, 19 (2) (2016), 717–736.
- [10] H. M. Akil, M. F. Omar, A. A. M. Mazuki, S. Safiee, Z. A. M. Ishak, and A. Abu Bakar, Kenaf fiber reinforced composites: A review, *Mater. Des.*, 32 (8–9) (2011), 4107–4121.
- [11] S. Wei Zhang, Green tribology: Fundamentals and future development, *Friction*, 1(2) (2013), 186–194.
- [12] S. Basavarajappa, G. Chandramohan, and J. Paulo Davim, Application of Taguchi techniques to study dry sliding wear behaviour of metal matrix composites, *Mater. Des.*, 28 (4) (2007), 1393–1398.
- [13] A. Mustafa, M. F. Bin Abdollah, H. Amiruddin, F. F. Shuhimi, and N. Muhammad, Optimization of friction properties of kenaf polymer composite as an alternative friction material, *Ind. Lubr. Tribol.*, 69 (2) (2017), 259–266.
- [14] C. W. Chin and B. F. Yousif, Tribological behaviour of Kfre composite, *Int. J. Mod. Phys. B*, 24 (28) (2010), 5589–5599.
- [15] C. W. Chin and B. F. Yousif, Adhesive and frictional behaviour of polymeric composites based on kenaf fibre, In *ICAT 274, 2nd Int. Conf. Adv. Tribol. 3-5 December 2008, Singapore*, 1–3.

The Effect of Graphite Loading as Reinforcement on Carbon Foam from Natural Resources

Nur Zaha Hassan^{1,a*}, Mohamed Nasrul Mohamed Hatta^{1,b},
Nur Azam Badarulzaman^{1,c} and Nurul Farahin Mohd Joharudin^{1,d}

¹Nano Structure and Surface Modification Research Group, Faculty of Mechanical and Manufacturing Engineering, Universiti Tun Hussein Onn Malaysia.

^agd190043@siswa.uthm.edu.my, ^bmnasrul@uthm.edu.my, ^cazam@uthm.edu.my,
^dfarahin.joharudin@gmail.com

Keywords: Graphite, Carbon Foam, Sucrose, Natural Resources, Mechanical Properties

Abstract. This study is to determine the effect of graphite as reinforcement material on natural resources carbon foam on the mechanical and physical properties. Sucrose is used as carbon precursor and graphite with various concentration from 0 wt% to 0.3 wt% was added into the carbon foam. Carbon foam was prepared by using template method followed by pre curing and carbonization process. Pre curing process was take place at 250°C and carbonization process was carried out at 900°C under inert atmosphere (using argon gas). The morphology, porosity, density and compressive strength were characterised in this experiment. Through Scanning Electron Microscope (SEM), graphite can be seen clearly embedded into the ‘window’ and fill the void space. Porosity of carbon foam decrease when the concentration of graphite increase and the density of carbon foam increase when the concentration of graphite increase. Carbon foam with 0.3 wt% graphite added shows the highest compressive strength (1.84 N/mm²) compared with carbon foam without graphite added (0.95 N/mm²). The properties of carbon foam are significantly influenced by the addition of graphite loading.

Introduction

In late 1960s, carbon foam was first developed by Walter Ford using phenol-formaldehyde as main carbon precursor [1]. Carbon foams are rigid and porous materials with certain attractive features like high temperature stability and lightweight which makes them versatile in many applications [2],[3]. Fabrication of carbon foam by fossil fuel based carbon precursors such as petroleum pitch and phenolic resin are now being depleted. Recently, the preparation of carbon foams is replaced by natural renewable resources, sucrose as the source of carbon is slightly increasing [4]. Sucrose has a highest carbon content and has been chosen as a famous carbon precursor for the preparation of carbon foam from natural resources material [4]. It is important for sustainable development by replace the petroleum based raw materials with natural renewable resources for the applications of industrial products.

Carbon foam from natural renewable resources has lower mechanical strength compared with carbon foam from petroleum or phenolic resin [5]. Not only that, carbon foam from natural resources also brittle in shape and has lower density. This situation happened because the formed of micro crack and voids inside the structure of carbon foam [6]. In order to overcome this problem, reinforcement material is needed to improve the quality strength of carbon foam. Besides, reinforcement material from carbon can helps to improve the carbon yield and also helps to improve the mechanical strength [7].

Material and Methods

Materials. Analytical reagent grade of sucrose (C₁₂H₂₂O₁₁), boric acid (H₃BO₃) and graphite were used in this experiment. Polyurethane foam (PU foam) with the density of 0.028g/cm³ were used as the template medium for the fabrication of carbon foam.

Methods. PU foam with the diameter of 30mm were washed with tap water to remove any dust or dirt and then were dry using an oven. Sucrose, boric acid, graphite with various concentration from 0 wt% to 0.4 wt% and distilled water were mixed homogeneously using magnetic stirrer. Distilled water is used to dissolve the mixture of powder until the mixture turns into slurry formed. Then, PU foam is dipped into slurry mixture until the slurry mixture fully dissolved into PU foam. Next, pre-curing and drying process takes place using an oven at 120°C before proceed to carbonization process. Carbonization process of the sample is done under inert atmosphere (argon gas) for 2 hours' dwell and heating rate at 2°C/min [6].

Characterization. Characterization in this experiment involved three properties which are morphology properties, physical properties and mechanical properties. The effect of carbon foam from different loading of graphite was investigated by several testing which is by Scanning Electron Microscope (SEM), porosity and density test and compression test.

Surface morphology and cell structure of carbon foam was observed by using Hitachi Scanning Electron Microscope (SEM) at 15 KV accelerating voltage without coating the specimen.

Porosity and density testing were used to investigate the physical properties. Archimedes method was used in these testing and the standard used are ASTM B962 [6]. Before testing, the samples are boiled into water for 2 hours and then soaked into distilled water for at least 12 hours.

For mechanical properties, the compression test was done on carbon foam with different loading of graphite. The compression test was guided by using ASTM C365 (year 2016) and Autograph AGS-X Series Universal Testing Machine (UTM) with the speed of the testing used is 0.5 mm/min [6].

Results and Discussion

Morphology. Figure 1 shows the surface morphology and cell structure of carbon foam with different graphite loading used: (a) no graphite added (b) 0.1 wt% (c) 0.2 wt% and (d) 0.3 wt% obtained by Scanning Electron Microscope (SEM). Micro crack and void can be seen clearly from figure 1(a) carbon foam without graphite added (only sucrose and boric acid). While in figure 1(b), 1 (c) and 1 (d), the graphite can be seen clearly embedded into the interconnected cellular structure and windows (cell wall to connect neighboring cells) which helps to avoid micro crack and void to form. When the concentration of graphite increases, the pore size of the cell wall becomes smaller. This is because the presence of graphite fills the void space and is embedded between the micro crack which formed a strong structure of carbon foam. It is interesting to discuss that graphite act as 'glue' to hold or repair the crack on the structure of carbon foam besides graphite is an ideal material. Figure 2 shows the shape and size of graphite used as reinforcement in carbon foam and the length of graphite use is between 11.1 - 33.1µm with flakes shape. The present of micro crack and void on the carbon foam can leads to brittle in strength and the increase of cell size which makes them easier to be broken [10].

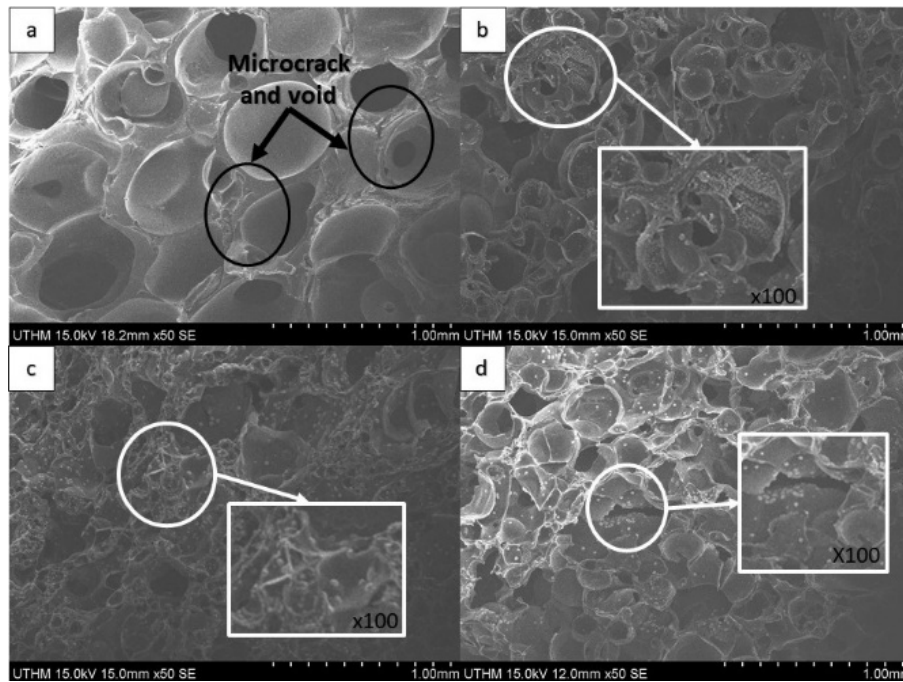


Fig. 1 SEM micrograph of carbon foam from different various of graphite loading (a) no graphite added (b) 0.1 wt% (c) 0.2 wt% and (d) 0.3 wt%

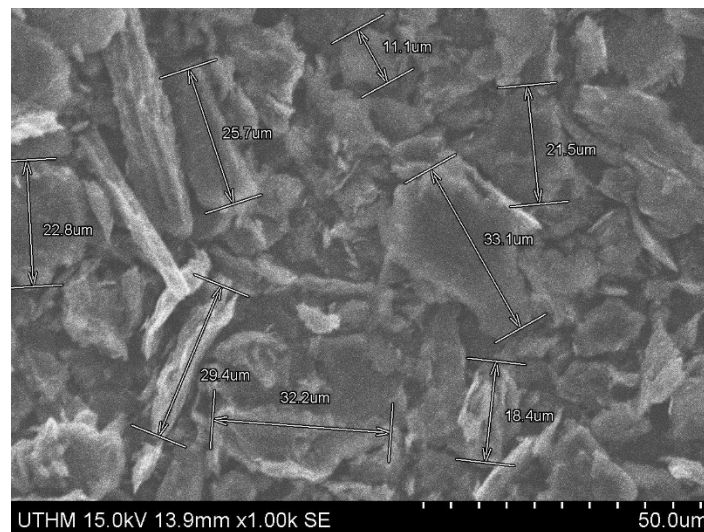


Fig.2 SEM micrograph of graphite that used as reinforcement on carbon foam

Physical Properties. Porosity and density test are used to investigate the potential physical properties of carbon foam. Figure 3 shows the density and porosity of carbon foam prepared at different graphite loading from 0 wt% to 0.3 wt%. Density of carbon foam increase when porosity of carbon foam becomes decrease. The density for carbon foam without graphite added is 3.17 g/cm^3 smaller density compared with graphite added which is 3.65 g/cm^3 (0.1 wt% graphite used). Then the density become increase when the concentration of graphite added increase. The present of graphite in carbon foam helps to reduce the micro crack and void between the window which makes the pore size become smaller which can be seen clearly through the SEM micrograph. Since then, the porosity result become smaller when the concentration of graphite increase. Percentage porosity of carbon foam without graphite is 67.15% and porosity of carbon foam with 0.3 wt% graphite is 56.93%.

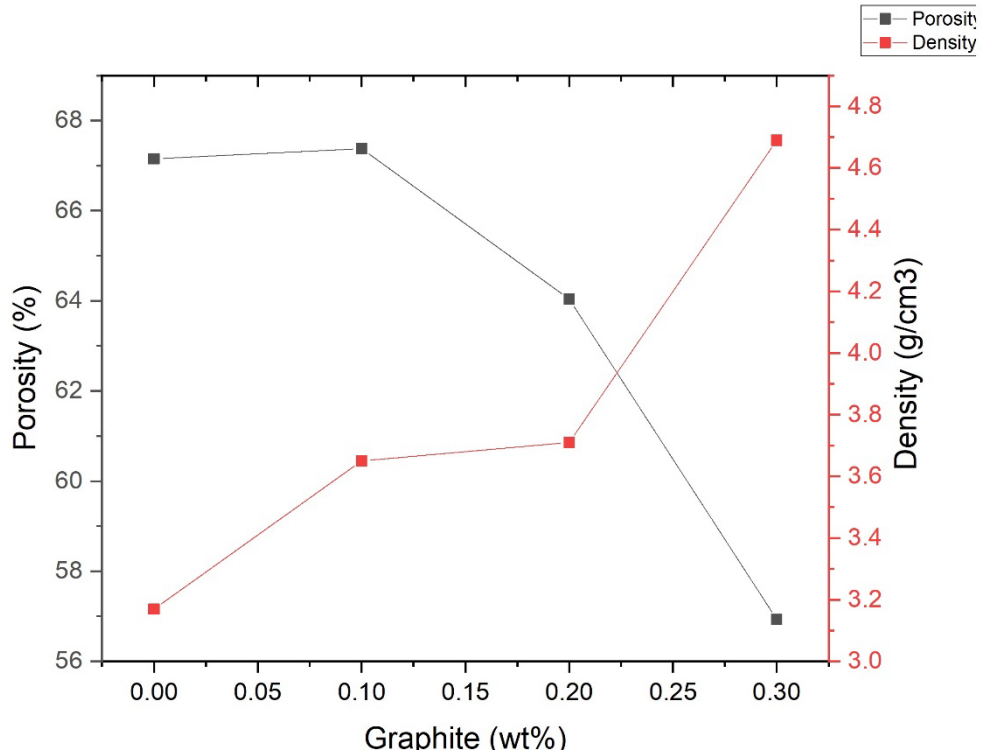


Fig. 3 Average density and porosity of carbon foam prepared at different graphite loading

Mechanical Properties. Figure 4 shows the compressive strength of carbon foam at different graphite loading (0 wt% to 0.3 wt%). The strength of carbon foam without graphite added is smaller compared to carbon foam with graphite added. The compressive strength of carbon foam without graphite is 0.95 N/mm^2 lower than carbon foam with 0.3 wt% graphite added which is 1.85 N/mm^2 . Graphite helps to prevent the micro crack and fill the void space and makes the structure of carbon foam much stronger. The present of micro crack and void on structure will leads to brittle in strength and cell size of structure becomes larger. Besides, graphite is basically strong fibers and also ideal material for reinforcement things [9]. The addition of graphite added influenced the strength of specimen since graphite is a good reinforcement material [8].

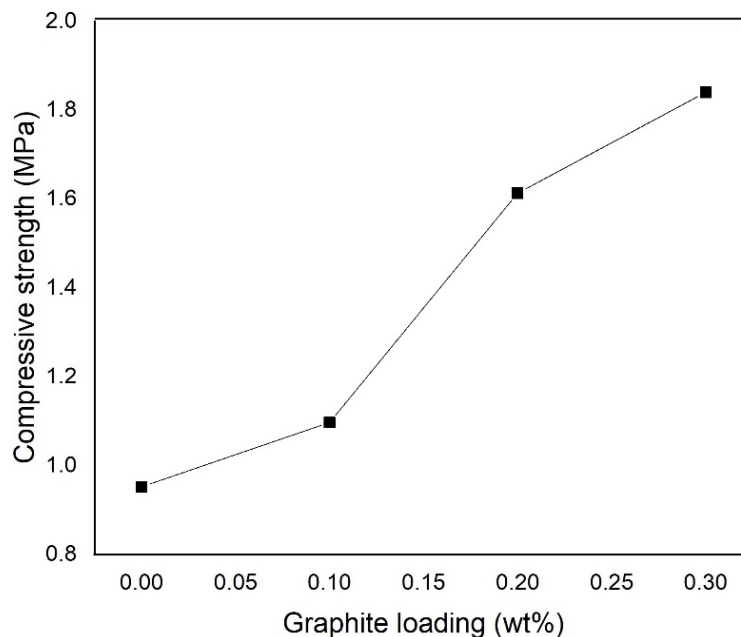


Fig. 4 Compressive strength of carbon foam at different graphite loading

Conclusions

Carbon foam from natural resources precursor with graphite as reinforcement material was successfully done by using template method. The effect of graphite was studied by several properties which are morphology properties (SEM), physical properties (porosity and density test) and mechanical properties (compression testing). Through SEM, the present of graphite fill the void space and embedded between the micro crack which formed a strong structure of carbon foam. The porosity and density result shows the trends when density of carbon foam increase, the porosity of carbon foam is decrease. Pore size of carbon foam reduce because the present of graphite embedded into the 'window' of the carbon foam. Density of carbon foam become increase when the addition of graphite is increase. For mechanical properties, the compressive strength increase when the addition of graphite increase. The highest compressive strength is 1.84 N/mm² at 0.3 wt% of graphite loading and carbon foam without graphite added shows the lowest strength which is 0.95 N/mm². The properties of carbon foam are significantly influenced by the addition of graphite loading. The objective of this paper is achieved when the graphite added leads to the improvement of the strength of the carbon foam and also graphite helps to reduce the microcrack and void on the carbon foam.

Acknowledgements

This research was supported by Ministry of Higher Education Malaysia through Fundamental Research Grant Scheme (FRGS/1/2018/TK03/UTHM/03/9). We also want to thank to Universiti Tun Hussein Onn Malaysia (UTHM) for sponsoring this work under research grant No. K050.

References

- [1] M.J.G. De Araujo, J. Villarroel-rocha, V.C. De Souza and K. Sapag, Carbon foams from sucrose employing different metallic nitrates as blowing agents: Application in CO₂ capture, *J. Anal. Appl. Pyrolysis*, 141(2019) 104-627
- [2] M. Inagaki, J. Qiu and Q.Guo, Carbon foam: Preparation and application, *Carbon N.Y*, 87(2015) 128-152
- [3] N. Afiqah, K. Kamarudin, N.Z. Hassan and M.N Mohamed, Effect of Carbonization Temperature on Physical and Mechanical Properties of carbon Foam, *Tech. Reports of Kansai University*, 62(2020) 3089-3096
- [4] R.Narasimman and K. Parabhakaran, Preparation of low density foams by foaming molten sucrose using an aluminium nitrate blowing agent, *Carbon N.Y*, 50(2012) 1999-2009
- [5] R.Narasimman, S. Vijayan and K. Prabhakaran, Carbon-carbon composite foams with high specific strength from sucrose and milled carbon fiber, *Materials Letters*, 144(2015) 46-49
- [6] N.Z. Hassan, M.Nasrul Hatta, N.A Badarulzaman and N.F Mohd, The effect of carbon whisker loading on carbon foam on physical and mechanical properties, *Tech. report of kansai*, 62(2020) 4593-4598
- [7] R. Narasimman, S. Vijayan, K.S. Dijith, K. P Surendran and K.Prabhakaran, Carbon composite foams with improved strength and electromagnetic absorption from sucrose and multi-walled carbon nanotube, *Mater. Chem. Phys*, 181(2016) 538-548
- [8] P.K. Kumari Archana, Analysis of graphite reinforced Aluminium-6061 Metal Matrix Composite using Stir Casting Method, *Research India Pub.* , 13(2018) 189-193
- [9] Hugh O. Pierson, *Handbook of Carbon, Graphite, Diamond and Fullerenes*, Noyes Publications, New Jersey, 1993.
- [10] R. Narasimman and K. Prabhakaran, Preparation of carbon foams with enhanced oxidation resistance by foaming molten sucrose using a boric acid blowing agent, *Carbon N.Y*, 55(2013) 305-312

Synthesis and Characterization of Palm Kernel Oil Polyol Based Shape Memory Polyurethane: Effect of Different Diisocyanates

NUR ATHIRAH Rasli @ Rosli^{1,a}, SYAZANA Ahmad Zubir^{1,b*}

¹School of Materials and Mineral Resources, Engineering Campus, Universiti Sains Malaysia, 14300 Nibong Tebal, Pulau Pinang, Malaysia

^anurathirahrasli@gmail.com, ^{b*}syazanazubir@usm.my

Keywords: shape memory polyurethane, crystallinity, hydrogen bonding, phase separation

Abstract. Shape memory polyurethane (SMPU) is a very versatile material that has a broad array of applications. The selection of soft segments and hard segments play critical roles in determining the structure-property behaviors of SMPU. This research was conducted to evaluate the role of distinct types of diisocyanate on the final properties of polyurethane (PU). Palm kernel oil polyol (PKO) based PU were produced by using two-step bulk polymerization method with variations of diisocyanates. Isophorone diisocyanate (IPDI), 4,4-methylenebis (cyclohexyl isocyanate) (HMDI) and hexamethylene diisocyanate (HDI) were used in the preparation of PU and the soft segment crystallinity, thermal and shape memory properties of the PU were evaluated. Based on the analyses, it was found that different types of diisocyanate and combination of diisocyanates had huge impact on the properties of the synthesized PU. The Fourier transformation infrared (FTIR) analysis revealed that IPDI based PU achieved the highest hydrogen bonding index value which promoted the phase separation. This is in accordance with differential scanning calorimetric (DSC) and x-ray diffraction (XRD) analysis which showed that IPDI based PU exhibited crystalline soft phase, hence resulted in an excellent shape fixity behavior. On the other hand, HDI and HMDI based polyurethane prepared showed absence of crystalline soft phase based on the DSC thermogram and XRD diffractogram. These results suggest the phase mixing phenomenon between soft and hard segments which contributed to low shape memory behavior of the resulting polyurethane.

Introduction

Shape memory polymers (SMPs) has become an interesting area in the revolution of polymer. They are well-known for their rapid response to external stimuli, ease of handling, and broad range of applications. They can return to their initial state from a temporarily deformed shape when triggered by stimuli [1, 2]. The external stimuli that can be used to trigger such reaction are electric field, thermal heating, magnetic field or photon energy [3]. Heat is commonly selected as external stimuli due to its simplicity during setting and known as thermo-responsive SMP. Thermo-responsive is the most existing SMPs which exhibit thermo-dependent performance.

One of the most common thermo-sensitive SMPs is shape memory polyurethanes (SMPUs) which often been used due to its wide-ranging sources and shape memory properties. SMPUs consist of two phase separated structures which are soft and hard segments. Soft segment is contributed by the polyol while hard segment is contributed by the reaction of diisocyanates and chain extender. The existence of hard segments offers mechanical strength that is accountable to memorize its initial shape after deformation. Meanwhile, soft segments store energy for dissipation, allowing polyurethane to revive to its original shape by the action of external stimuli [4].

SMPU properties can be customized depending on a variety of factors, including molecular weight and type of soft segment, symmetry and type of hard segment, and chain extender which will essentially affect the morphology-property relationships. Yilgor and coworkers have systematically reported the study of thermoplastic PU using various diisocyanate (1,4-phenylene (PPDI), 1,3-phenylene (MPDI), 4,4'-methylenediphenyl (MDI), 4,4-methylenebis (cyclohexyl isocyanate) (HMDI), 2,4-tolylene (TDI), trans-1,4-cyclohexyl (CHDI) and hexamethylene (HDI)) with poly(tetra methylene oxide) (PTMO) as soft segments without the use of chain extender [5-8]. PU produced

using symmetric diisocyanates and urea as hard segments showed superior microphase separation, crystallinity, good mechanical behaviour and elastomeric properties as compared to unsymmetrical MPDI, TDI and HMDI. However, the authors have not explored the potential of shape memory characteristics of the PU.

Hence, this experiment was carried out to examine the impact of various diisocyanates 4,4-methylenebis (cyclohexyl isocyanate) (HMDI), hexamethylene diisocyanate (HDI) and isophorone diisocyanate (IPDI) on the properties of SMPU. Polycaprolactone diol (PCL) was used as the soft segment throughout this work since it facilitates crystallization [9]. Due to environmental concerns, PKO was introduced into this system. In addition, PKO also acts as plasticizer to improve chain flexibility.

Materials and Methods

PKO (MW of 1000 g/mol) was provided by Universiti Kebangsaan Malaysia (UKM). Meanwhile, PCL (MW of 2000 g/mol), HMDI (MW of 262.35 g/mol), HDI (MW of 168.19 g/mol), IPDI (MW of 222.28 g/mol), 1, 4-butanediol (BD) (MW of 90.12 g/mol) and dibutyltin dilaurate (DBTDL) were all procured from Sigma Aldrich.

Preparation of PU. PU was produced using two-step bulk polymerization method by incorporating different types of diisocyanates which are HMDI, IPDI, HDI and a mixture of HMDI and IPDI together with PCL 2000. The synthesis of PU involves the use of PKO based polyol with the addition of BD as chain extender and DBTDL as catalyst for the overall reaction. Firstly, polyol and diisocyanates were poured into a three-neck flask assembled together with a mechanical stirrer, thermometer, heating oil bath and N₂ inlet and outlet. The mixture was allowed to react for 2.5 hours with temperature of 80°C. In order to form the prepolymer, PKO was added into the mixture and the reaction was continued for 2 hours. The rate of stirring used during the synthesis was in the range of 190-200 rpm. In the second step, BD and DBTDL were added to the prepolymer in the internal mixer at 90°C for 15 minutes. The PU samples were then compression molded at 160°C into a 0.5 mm thick sheets.

Characterization Techniques. Fourier Transform Infrared (FTIR) was performed to investigate the characteristic bands and hydrogen formation present in PU. The spectral resolution used was 4 cm⁻¹ in the range of 600 cm⁻¹ to 4000 cm⁻¹ wavelengths with 32 scan number. The carbonyl group region was studied in detail in order to obtain more information on hydrogen bonding formation. The carbonyl (C=O) stretching area was deconvoluted using Fityk 0.9.8 software by applying Gaussian transformation. The hydrogen bonding index (HBI) and the degree of phase separation (DPS) value was calculated by using Eq. 1 and Eq. 2.

$$\text{HBI} = \frac{\sum \text{AHCO}}{\sum \text{AFCO}} \quad (1)$$

$$\text{DPS} = \text{HBI} / (1 + \text{HBI}) \quad (2)$$

Where $\sum \text{AHCO}$ and $\sum \text{AFCO}$ are the total areas under hydrogen bonded and free carbonyl bands, respectively.

Differential scanning calorimeter (DSC) Mettler Toledo, Perkin Elmer analysis was carried out to determine thermal behaviour of the PU. 5-10 mg samples were secured in aluminium crucible pans. Single thermal scan was conducted starting from room temperature (RT) to 160°C at a scan rate of 10°C/min. The percentage of crystallinity, X_c of the PUs are determined based on Eq. 3.

$$X_c = \Delta H_m / (\Delta H_m^\circ) \quad (3)$$

Where, ΔH_m° is the heat of fusion of 100% crystalline PCL (139.5 Jg⁻¹) and ΔH_m is the heat of fusion of the polymer under investigation.

X-ray diffractogram (XRD) was performed using a Bruker AXS D8 Advance diffractometer. The sample was prepared with a dimension of 10 x 10 x 0.5 mm before irradiated with X-rays using Cu-K α x-ray source and the angular ranging from (2θ) of 10° to 40°.

In order to evaluate the shape memory effect of PU, a shape memory test was conducted. The sample was prepared using the same method as described by Rasli and Ahmad Zubir [10]. Eqs. 4 and 5 were used to calculate the percentage of shape fixity and shape recovery.

$$\text{Shape fixity (\%)} = (\theta_{cr}/90^\circ) \times 100 \quad (4)$$

$$\text{Shape recovery (\%)} = ([90^\circ - \theta_f]/90^\circ) \times 100 \quad (5)$$

Where, θ_{cr} is angle of removal load and θ_f is final angle.

Results and Discussion

FTIR Analysis. Fig. 1 presents the FTIR spectra of PU prepolymer and PU. From Fig. 1 (a), it can be observed that the -NCO peak of prepolymer appeared at around 2265 cm^{-1} for all samples. The broad peak in FTIR spectrum at approximately 3440 cm^{-1} indicate the overlapping of OH and N-H groups. The N-H peak appeared due to the formation of urethane linkages as OH groups of polyols reacted with -NCO group of diisocyanates. The band at 2937 cm^{-1} is designated to asymmetric -CH_2 and the stretching at 2862 cm^{-1} is assigned to symmetric -CH_2 . The peak observed at 1726 cm^{-1} is due to the stretching of carbonyl group (C=O) vibrations of the polyester polyols in prepolymer. The band at 1238 cm^{-1} is attributed to asymmetric C-O-C stretching [11]. Meanwhile for PU sample, OH peak is overlapped with NH peak in the spectra at the range of $3200 - 3600 \text{ cm}^{-1}$ as shown in Fig. 1 (b). Apart from that, the complete reaction of urethane linkages is indicated by the disappearance of -NCO group in the range of $2200\text{-}2300 \text{ cm}^{-1}$.

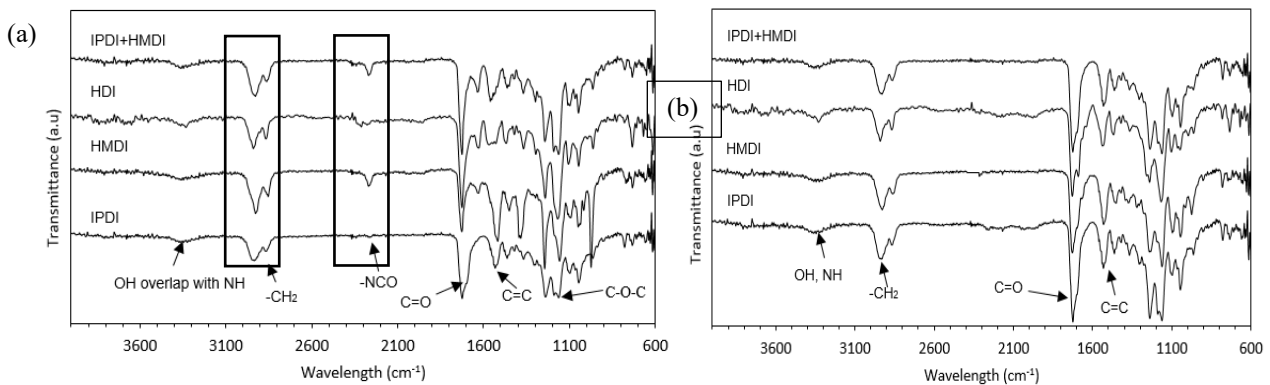


Fig. 1: FTIR spectra of (a) prepolymer and (b) polyurethane of PU samples

From Table 2, both HMDI and HDI based PU has the DPS value of 0.4 while IPDI and IPDI+HMDI based PU has the value of 0.7 and 0.6 respectively. IPDI and IPDI+HMDI based PU samples showed high HBI value caused by an increase in hydrogen-bonded urethane groups [12] which led to the formation of hard segment domains. Consequently, the phase separation occurred which promoted the occurrence of soft segment crystallization. This is in accordance with the DSC analysis which will be discussed in the next section. The high DPS value obtained suggest the phase separation phenomenon while the low DPS values is corresponded to the phase mixing of both hard and soft segments in PU [13].

Table 2: HBI and DPS value of PU samples

Sample	Band I F-CO (cm ⁻¹)	Band II H-CO (cm ⁻¹)	Band III H-CO (cm ⁻¹)	Band IV H- CO (cm ⁻¹)	HBI	DPS
IPDI	1731	1694	1667	1633	2.17	0.7
Area	1.03	1.20	1.04	0.13		
HMDI	1731	1692	1663	1633	0.75	0.4
Area	2.29	1.20	0.51	0.10		
HDI	1727	1694	1660	1641	0.64	0.4
Area	4.03	1.94	0.64	0.30		
IPDI+HMDI	1721	1688	1669	1646	1.63	0.6
Area	0.43	0.45	0.25	0.14		

DSC Analysis. The thermal properties of the PU samples were investigated using DSC analysis. The scan curves of the PU samples are shown in Fig. 2 while Table 3 summarized all the data measurements obtained in this characterization. Based on the results, only IPDI based PU and mixture of IPDI and HMDI based PU reveal an obvious endothermic peak in the range of 42.4 to 45.6°C which is attributed to the melting temperature, T_m of PCL soft segment which indicates the occurrence of phase separation in those samples. PU synthesized using IPDI demonstrate higher ΔH_m as compared to mixture of IPDI and HMDI based PU, implying the presence of more soft segment crystalline structure in the sample. In addition, there is no trace of endothermic peak present in HMDI based PU sample. Hence, suggesting that the use of IPDI instead of HMDI promoted the crystallization of PCL soft segments. HMDI and HDI based PU did not exhibit endothermic behaviour which is assigned to the melting of the crystalline soft phase. The possible reason for this is the occurrence of phase mixing of soft and hard segments which caused the disruption of soft segment crystallinity [14].

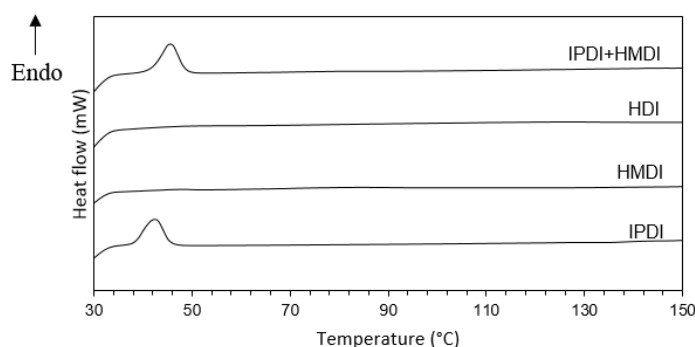


Fig. 2: DSC thermograms of PU prepared using different diisocyanates

Table 3: Thermal characteristic of PU prepared using different diisocyanates

Sample	T_m (°C)	ΔH_m (J/g)	Crystallinity (%)
IPDI	42.4	30.2	21.6
HMDI	-	-	-
HDI	-	-	-
IPDI+HMDI	45.6	26.1	18.7

XRD Analysis. The typical XRD curves in Fig. 3 shows two prominent peaks around $2\theta = 21.7^\circ$ and 23.8° . Both peaks are corresponded to the crystalline structure of the PCL soft segments [15]. The intensity of the peaks for PU synthesized using IPDI was the highest followed by combination of IPDI and HMDI based PU. This shows that the soft segment crystallinity of the PU polymer was promoted with the use of IPDI as diisocyanate. The incorporation of IPDI in PU system will produce a semicrystalline soft segments and lead to the formation of more hard segment domains, hence promote the microphase separation in the PU sample. Meanwhile, the other two samples, HMDI and HDI based PU for both series did not show obvious peaks indicating the soft segment was amorphous which follows the DSC analysis. The decreased of the peak intensity of these two samples can be

explained in terms of the restrictions introduced by the presence of strong inter-chain interactions through hydrogen bonding [16]. As a result, the PCL soft segments tend to become more amorphous rather than semi-crystalline as achieved by HMDI and HDI based PU in this study.

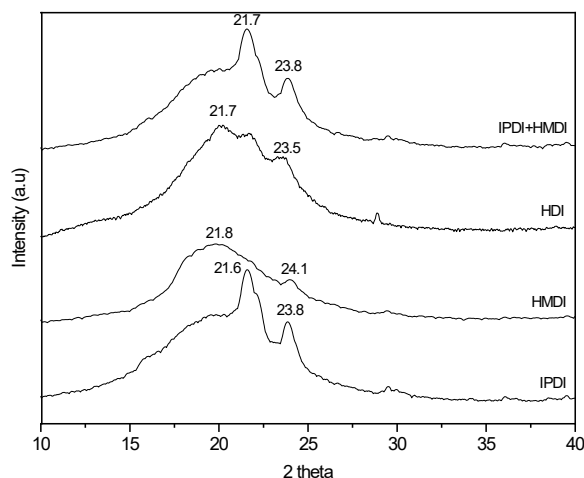


Fig. 3: XRD patterns of PU prepared using different diisocyanates

Shape memory behaviour. Shape memory properties of the synthesized PU is summarized in Table 4. As can be seen from the table, all of the PU samples exhibit 100% shape recovery. The high shape recovery is due to strong bonding between physical crosslinks in hard segment domains [17]. The shape fixity for all of the synthesized PU is in the range of 35.2-93.7%, depending on the type of diisocyanates used in preparing the sample. PU prepared using IPDI has the highest shape fixity of 93.7% whereas the lowest was achieved by HDI based PU with the value of 35.2%. The shape fixity characteristics observed in this study are influenced by the presence of soft segment crystalline structure to fix the temporary shape via cooling. This can be confirmed by observing the XRD and DSC analyses in which the IPDI based PU sample has successfully achieved high soft segment crystallinity which leads to high shape fixity behaviour. This is due to the ability of IPDI to provide higher degree of phase separation. Meanwhile, the low shape fixity of HDI based PU is due to the low soft phase crystallinity which leads to the decrease capacity to fix the temporary shape. This is in consistent with the data discussed in DSC analysis, which have shown that no crystalline soft phase is detected in the scan curves.

Table 4: Shape memory properties of PU

Sample code for polyurethane	Shape fixity (R_f) (%)	Shape Recovery (R_r) (%)
IPDI	93.7	100
HMDI	70.4	100
HDI	35.2	100
HMDI + IPDI	74.8	100

Summary

In this study, PKO based PU was successfully prepared via two-step polymerization method using different types of diisocyanates. Based on the analyses, it was found that the use of different types of diisocyanates and combination of diisocyanates had great impact on the properties of the synthesized PU. The result discussed in this study revealed that IPDI based PU exhibit better performance in terms of thermal and shape memory properties as compared to HMDI and HDI based PU. IPDI based PU possessed highest HBI value and hence achieved high DPS value which correspond to the formation of microphase separation in PU. DSC and XRD analyses have shown that the IPDI based PU exhibited crystalline soft phase which resulted in the highest shape fixity value. Excellent shape recovery value is obtained for all samples suggesting the presence of strong physical crosslinks among the hard segment domains.

Acknowledgement

The authors would like to thank Ministry of Higher Education Malaysia for Fundamental Research Grant Scheme with Project Code: FRGS/1/2019/TK05/USM/03/2 for funding this research work.

References

- [1] W. M. Huang, Y. Zhao, C. C. Wang, Z. Ding, H. Purnawali, C. Tang, and J. L. Zhang, Thermo/chemo-responsive shape memory effect in polymers: A sketch of working mechanisms, fundamentals and optimization, *J. Polym. Res.* 19(9) (2012) 9952.
- [2] W. Small IV, P. Singhal, T. S. Wilson, and D. J. Maitland, Biomedical applications of thermally activated shape memory polymers, *J. Mater. Chem.* 20(17) (2010) 3356–3366.
- [3] H. Wang, J. Yu, H. Fang, H. Wei, X. Wang, and Y. Ding, Largely improved mechanical properties of a biodegradable polyurethane elastomer via polylactide stereocomplexation, *Polymer* 137 (2018) 1-12.
- [4] A. Lendlein, and S. Kelch, Shape-memory polymers. *Angewandte Chemie International Edition*, 41(12) (2002) 2034–2057.
- [5] J.P. Shehth, D.B. Klinedinst, G.L. Wilkes, Y. Iskender, and I. Yilgor, Role of chain symmetry and hydrogen bonding in segmented copolymers with monodisperse hard segments, *Polymer* 46 (18) (2005) 7317-22.
- [6] D.B. Klinedinst, E. Yilgor, I. Yilgor, F.L. Beyer, J.P. Sheth, and G.L. Wilkes, Structure property behaviour of new segmented polyurethanes and polyureas without use of chain extenders, *Rubber Chem. Technol.* 78(5) (2005) 737-53.
- [7] S. Das, D.F. Cox, G.L. Wilkes, D.B. Klinedinst, I. Yilgor, E. Yilgor, et al., Effect of symmetry and H-bond strength of hard segments on the structure-property relationships of segmented, nonchain extended polyurethanes and polyureas, *J. Macromol. Sci. Part B Phys.* 46(5) (2007) 853-75.
- [8] S. Das, I. Yilgor, E. Yilgor, B. Inci, O. Tezgel, F.L. Beyer, et al., Structure-property relationships and melt rheology of segmented, non-chain extended polyureas: effect of soft segment molecular weight, *Polymer* 48(1) (2007) 290-301.
- [9] F. Li, Y. Chen, W. Zhu, X. Zhang, and M. Xu, Shape memory effect of polyethylene/nylon 6 graft copolymers, *Polymer* 39 (1998) 6929-6934.
- [10] N. A. Rasli, and S. A. Zubir, Synthesis and characterization of ipdi based shape memory polyurethane, *Mater. Sci. Forum* (2020) 142–147.
- [11] A. Khosravi, and M. Sadeghi, Separation performance of poly (urethane – urea) membranes in the separation of C2 and C3 hydrocarbons from methane, *J. Membr. Sci.* 434 (2013) 171–183.
- [12] S. M. Cakić, I. S. Ristić, I. Krakovský, D. T. Stojiljković, P. Bělský, and L. Kollová, Crystallization and thermal properties in waterborne polyurethane elastomers: Influence of mixed soft segment block, *Mater. Chem. Phys.* 144(1–2) (2014) 31–40.
- [13] N. H. Trinh, M. Jaafar, C. X. Viet, and S. A. Zubir, Palm kernel oil polyol based shape memory polyurethane: effect of polycaprolactone and polyethylene glycol as soft segment, *Mater. Res. Express* 7(2) (2020) 025704.
- [14] Z. S. Petrović, and I. Javni, The effect of soft-segment length and concentration on phase separation in segmented polyurethanes, *J. Polym. Sci. B Polym. Phys.* 27(3) (1989) 545–560.
- [15] X. Jing, H. Y. Mi, H. X. Huang, and L. S. Turng, Shape memory thermoplastic polyurethane (TPU)/poly(ϵ -caprolactone) (PCL) blends as self-knotting sutures, *J. Mech. Beh. Biomed. Mater.* 64 (2016) 94–103.
- [16] M. V. Pergal, V. V. Antic, S. Ostojic, Marinovic-Cincovic, and J. Milena Djonlagic, Influence of the content of hard segments on the properties of novel urethane-siloxane copolymers based on a poly (ϵ -caprolactone) triblock copolymer, *J. Serb. Chem. Soc.* 76(12) (2011) 1703–1723.
- [17] Y. Q. Fu, W. Huang, M., J. K. Luo, and H. Lu, Polyurethane shape-memory polymers for biomedical applications, *Shape Memory Polymers for Biomedical Applications*, (2015) 167–195.

Characterization of Sodium Alginate Membrane Plasticized by Polyols and Polyamine for DMFC Applications

MARYAM TAUFIQ Musa^{1,a}, NORAZUWANA, Shaari^{1,b*}
and SITI KARTOM, Kamarudin^{1,2,c}

¹Institute of Fuel Cell, Universiti Kebangsaan Malaysia, 43600, Selangor, Malaysia

²Faculty of Engineering & Built Environment. Universiti Kebangsaan Malaysia, 43600, Selangor, Malaysia

^amaryam843@outlook.com, ^{b*}norazuwanashaari@ukm.edu.my, ^cctie@ukm.edu.my

Keywords: polyols, polyamine, characterization, plasticizer, sodium alginate, membrane, composite, direct methanol fuel cell (DMFC)

Abstract. This study reports the effect of plasticizers namely isopropanol, polyethylene glycol, maltitol and spermidine on the properties of the sodium alginate composite membrane. The concentration of each potential plasticizer was set at minimum to execute performance. Properties of sodium alginate were studied through characterization studies - Field Emission Scanning Electron Microscope (FESEM) to observe on the morphology structure. The membrane performance is also seen through water uptake and swelling ratio tests. Isopropanol produced better plasticizer with the lowest water uptake of 575.53% and less hydrophilic compared to spermidine (1268.46%), polyethylene glycol (1014.30%) and maltitol (595.82%). Further study may require copolymerization to support polyol for ensuring structure firmness. This study proven the plasticizers could enhance membrane's flexibility in DMFC and becoming a promising choice of additives for better alginate-based membrane establishment.

Introduction

Alginate is a prominent water-soluble polysaccharide found in brown seaweed. It consists of (1-4)-linked b-D-mannuronic acid (M) and a-L-gluronic acid (G) units. Alginates have a number of advantageous properties, including excellent biocompatibility, non-toxicity, non-immunogenicity, biodegradability, relatively low costs and easy combination with divalent cations (e.g. calcium) [1]. Alginate can be manufactured into a variety forms, such as film, microspheres and fibers, because of their reversible solubility [2-4]. Alginate has a six-membered ring structure backbone; therefore, it is difficult to increase the rigidity or to compact. This structure creates larger void volumes and allows the absorption of water molecules. Unfortunately, excessive water absorption causes membrane swelling and thereby decreases membrane selectivity [5]. It is very important to balance between membrane permeability and selectivity to water or gas. To address this shortcoming, alginate has been modified using various methods, which can be categorized as covalent crosslinking, ionic crosslinking, and non-bond interactions [6]. Ionic crosslinking provides better results because the produced polymer electrolyte complex is both robust and hydrophilic [1], [7]

The moisture content in a polymer-based film could induce significant changes in their structure as well as properties [5], [9-12] besides can be affected also by the addition of these polyols – isopropanol, polyethylene glycol and maltitol which are hydrophilic plasticizers. The role of plasticizers in a non-Nafion based membrane, is to improve the film flexibility and reducing brittleness [13]. Isopropanol was chosen due to its ability to dehydrate – mitigating the water sorption [14], [15]. Polyethylene glycol was chosen due to its flexible structure [16] while maltitol was chosen due to its high molecular weight, which could display high rheological properties [17]. Due to polyamine spermidine has been studied for its hygroscopicity potential and able to affect morphological and barrier properties of protein-based films [18], the present study will find out the potential among the polyols. However, no specific research involving isopropanol, polyethylene glycol, maltitol and spermidine, been used as plasticizer for alginate film. This work will investigate

the influences of three different polyols and spermidine on the microstructure and properties of sodium alginate films in ambient states, which beneficial for executing of sodium alginate as flexible membrane fuel cell application.

Materials and Methods

Materials. Synthetic sodium alginate ($(C_6H_9NaO_7)_n$) powder, spermidine ($C_7H_{19}N_3$, $\geq 99\%$), maltitol ($C_{12}H_{24}O_{11}$, $\geq 98\%$), and chemically pure polyethylene glycol (PEG 400, $(C_2H_4O)_nH_2O$) were purchased from Sigma Aldrich while isopropanol (C_3H_8O , $\geq 99.7\%$) and calcium chloride ($CaCl_2$, $\geq 99.5\%$) were obtained from R&M chemicals. These chemicals were used as received without further purification. Deionized water through a Millipore system (Milli-Q) was used in all experiments. Wisd ultrasonic cleaner, JEIO-Tech convection oven and Carbolite chamber furnace were the equipment utilized together along the preparation of samples process.

Preparation of the plasticized membrane. The biopolymer membrane was made of 1.5 wt% sodium alginate with deionized water as the solvent. The membrane was crosslinked internally using 1ml of 1.5 wt% of calcium chloride dropwise alternately with 1ml of four different plasticizers after sodium alginate powder had fully dissolved in the solution. The four plasticizers used were 2% spermidine, 5% isopropanol, 2% maltitol and 2% polyethylene glycol. Air bubbles was concerned to be avoided its occurrence along the preparation otherwise sonicator is required to overcome it. The samples were heated up to 70 °C for 12 hours duration. The control which consisted of pure sodium alginate was undergone the same procedures as well. The notation for the samples is as assigned in Table 1 below.

Table 1: Assignment of samples

Membrane matrix	Crosslinking agent	Plasticizer	Notation as
Sodium Alginate	-	-	SA1
Sodium Alginate	Calcium chloride	Isopropanol	SA2
Sodium Alginate	Calcium chloride	Spermidine	SA3
Sodium Alginate	Calcium chloride	Polyethylene glycol	SA4
Sodium Alginate	Calcium chloride	Maltitol	SA5

Characterization. The samples and the control were characterized using analytical instrument, namely FESEM, which was considered for the samples' morphology observation, pore size and shape observations.

Performance tests (water uptake and swelling ratio). The samples were fully soaked in deionized water for 24 hours at room temperature. Each of them including the pure sodium alginate were observed in different containers. The samples were proceeded to drying process for 60 minutes at 60 °C. The weight of the samples were taken and recorded before, W_{wet} and after, W_{dry} the drying step. Meanwhile, swelling ratio test was carried out similarly like the water uptake test, but with the length measurement of the membrane replacing the weight readings. The length of the membrane samples after the immersion denoted as L_{wet} and the length of the dried membrane denoted as L_{dry} .

Results and Discussions

Physical Observations. The membrane film samples were transparent-looking appearance and less flexibility such that it could be break apart with bare hands before proceeded to external crosslinking. Fig. 1 showed SA1-5 prepared in petri dish after membrane filming.

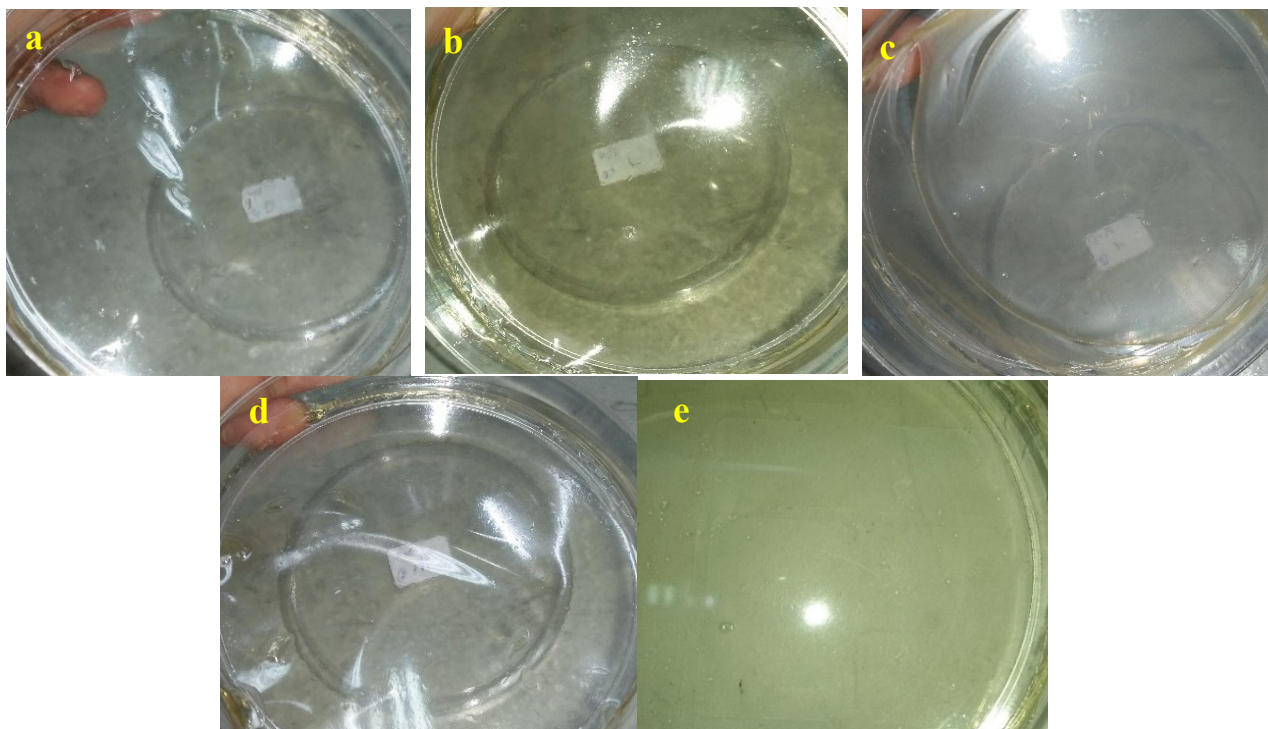


Fig. 1: Sodium alginate-based membrane samples of SA2 (a), SA3 (b), SA4 (c), SA5 (d) and control sample, SA1 (e) after heated up to 70 °C for 12 hours for membrane filming.

Scanning Electron Microscopy (SEM). The surface morphology and microstructure of the sodium alginate-based membranes were characterized by SEM as shown in Fig. 2. It is clearly could be seen that the addition of polyols and polyamine gave high influence on the surface of the membrane matrix, turning it up to rougher microstructure. SA5 showed more homogeneous and smoother surface than SA4, but SA4 looked much denser when scaled to larger magnification as if no free voids or big pores could be seen. Smaller micropores could be seen in SA5, implying that the plasticizer (maltitol) could enhance the water absorption which might result to film fragility and swollen. SA2 was found has interlayer surfaces than SA4, depicting the hydroxyl group of the plasticizer (isopropanol) successfully form hydrogen bonding interaction with the alginate matrix [19]. Polyamine in SA3 affecting the membrane to have very rough surface with tiny particles deposited causing agglomeration, denoting that the amino group at the end of spermidine backbone not forming strong interaction with the polymer matrix [13], [20]. Interlayer surface shown by SA2 could provide higher flexibility as polymer electrolyte membrane compared to the rests. These features, interlayer surface and dense microstructure could assure that water molecules or ions could be diffused in with small amount, hence impacting the membrane to be flexible, without easily break apart and performing smooth performance for DMFC operation.